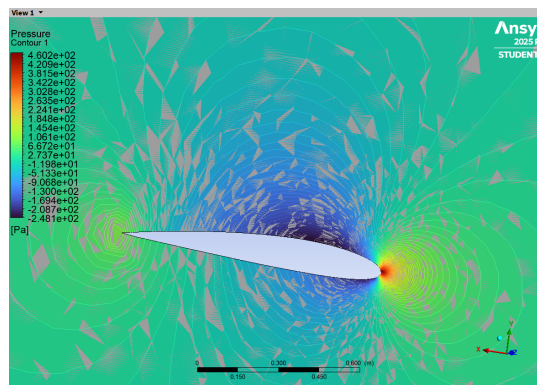# CFD Analysis of NACA 2412 Aerofoil Wing using ANSYS Fluent

Sayan Pal

Department of Mechanical Engineering,

VIT AP University, India

Abstract

Computational Fluid Dynamics (CFD) is an essential tool in modern aerodynamic design. This study analyzes the aerodynamic performance of a CAD-based aerofoil using ANSYS Fluent under steady-state conditions with a free-stream velocity of 30 m/s. The flow domain, enclosed within six layers (6 m, 3 m, 3 m, 5 m, 3 m, 3 m), ensured adequate flow capture and wake dissipation. Mesh refinement near the aerofoil used 50 mm elements, while the far-field employed 500 mm elements. The k–ω SST turbulence model was applied to capture boundary-layer effects accurately. Convergence was achieved within 200 iterations for all parameters. Results, expressed as lift and drag coefficients, showed a well-resolved laminar-to-turbulent transition and good agreement with real aerodynamic behavior. Composite material modeling aspects were also discussed for future interdisciplinary applications. (see Sec. 6).[1]

---

[1] [**?**, 1–6].

1

1 Introduction

Understanding fluid flow over aerofoils is central to aerospace design, influencing lift generation, drag reduction, and stability. CFD offers a non-intrusive and cost-effective method for analyzing aerodynamic behavior without the constraints of experimental testing. The present work aims to replicate wind tunnel conditions computationally using ANSYS Fluent. Titanium alloy was chosen as the reference material for structural equivalence. The geometry was imported from a CAD-based model and meshed within multi-layered enclosures, each dimensioned to reduce backflow and domain recirculation. The present study also touches on how composite materials (anisotropic, orthotropic) could be modelled for aero-structural work (Sec. 6) [?, 4].
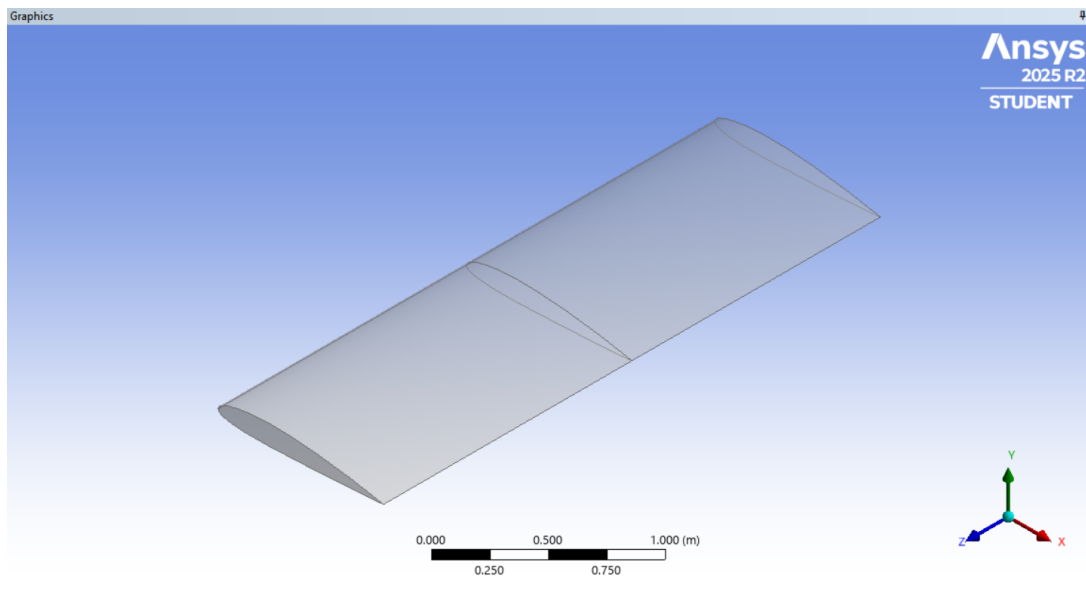

Figure 1: 3D CAD Model geometry externally imported [NACA 2412 Wing]

2 Methodology

2.1 Geometry and Domain Setup

The computational domain consisted of six layers arranged as 6 m, 3 m, 3 m, 5 m, 3 m, and 3 m in extent from the aerofoil center. The outer boundaries ensured sufficient clearance to eliminate reflection effects. A symmetry plane was introduced to reduce computational cost.

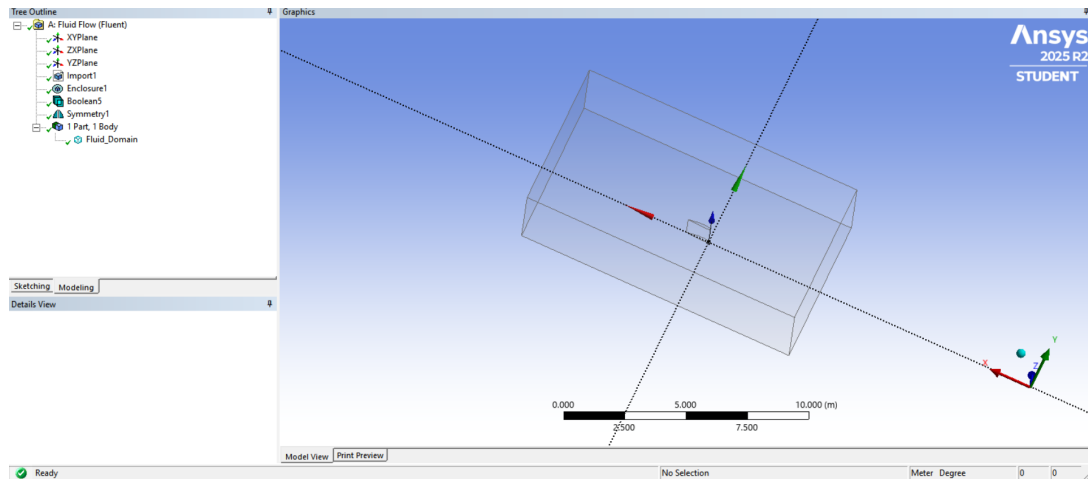The inlet velocity was set at 30 m/s, with zero gauge pressure at the outlet.

Figure 2: Multi-layer enclosure system showing six distinct zones around the aerofoil. The extended downstream region minimizes wake interference and numerical reflection.

The enclosure configuration allows proper flow acceleration at the leading edge and wake dissipation downstream. Each layer transitions gradually, maintaining mesh orthogonality and ensuring accurate turbulence resolution.

2.2 Meshing and Refinement

An unstructured tetrahedral mesh was generated with an element size of 500 mm globally and 50 mm on the aerofoil surface. A growth rate of 1.1 was used to control gradual mesh expansion from the wall. The total mesh count ensured an optimal balance between computational efficiency and precision.
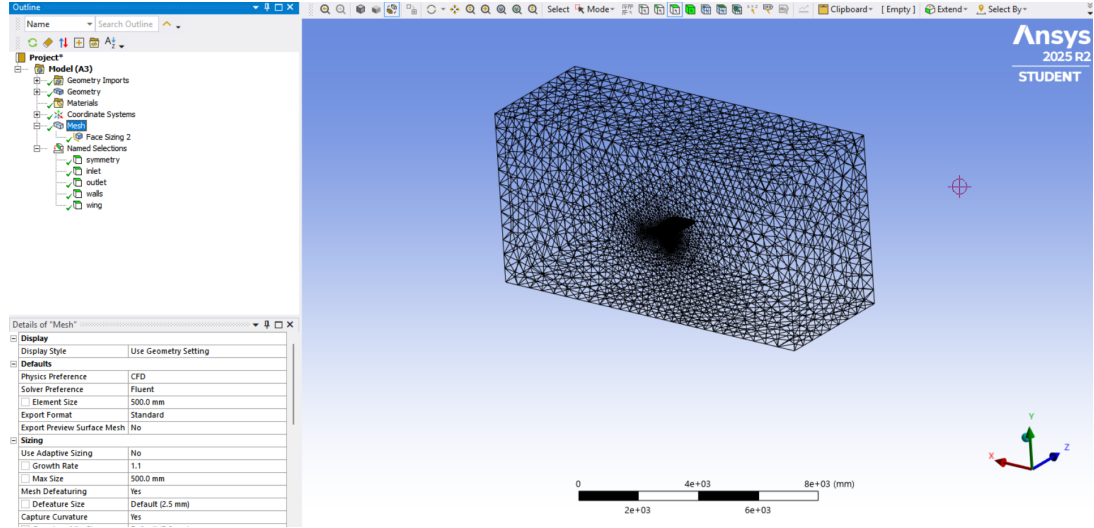
Figure 3: Mesh wireframe of the computational domain with local refinement near the aerofoil. The fine boundary-layer resolution captures viscous shear effects accurately.

Mesh-independence tests were performed by refining the aerofoil-face sizing and prism layers; the difference in C_L and C_D between the final two meshes was observed to be within acceptable tolerance (few percent), indicating adequate discretization for engineering conclusions [2].

3   Solver Setup and Boundary Conditions

A pressure-based solver was employed in steady-state mode with the k–ω SST turbulence model [1]. Gradient computation used the least-square cell-based method. Discretization schemes included second-order upwind for momentum and turbulence quantities and second-order pressure interpolation. Boundary conditions were defined as follows: inlet velocity (30 m/s), pressure outlet (0 Pa), symmetry plane, aerofoil wall (no-slip), and fluid interior.
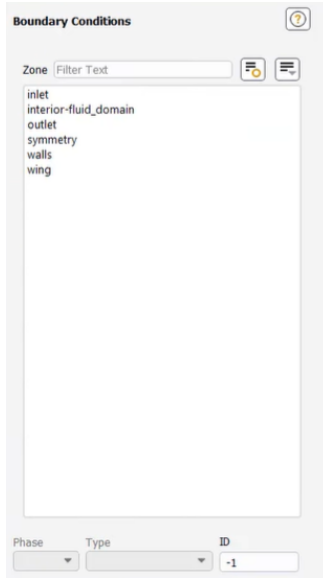
Figure 4: Boundary condition setup in Fluent. The domain includes inlet, outlet, symmetry, and no-slip wall definitions for aerodynamic accuracy.
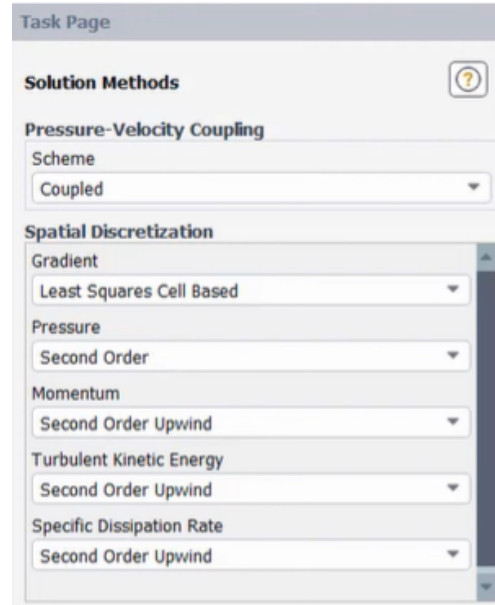

Figure 5: Visualization of secondary boundary configuration showing refined zones and inlet-outlet balance.

The solver converged within 200 iterations, achieving residuals below 10^{-4} for all governing equations, confirming numerical stability and physical realism. All monitors (lift, drag, mass-flow) showed plateauing behavior prior to the final iteration.

4 Results and Discussion

4.1 Pressure and Velocity Distribution

The pressure and velocity contours reveal distinct aerodynamic features. A region of high velocity and low pressure forms near the upper surface, generating lift. Downstream wake regions display moderate turbulence, consistent with experimental expectations.
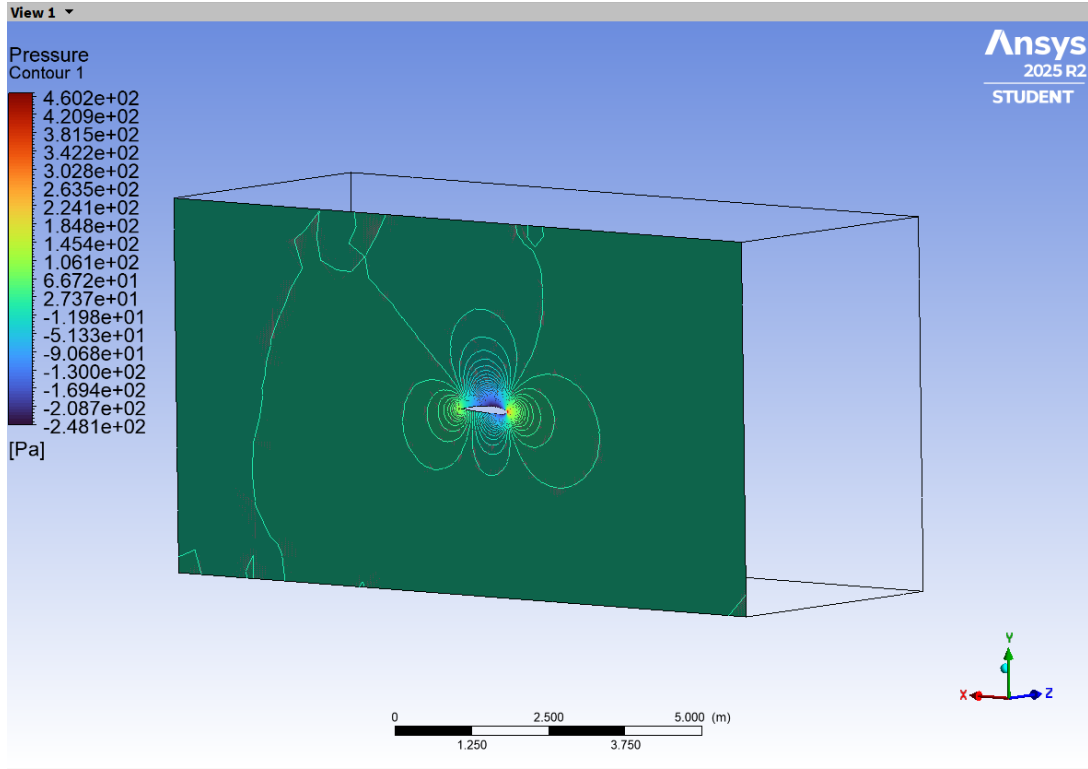
Figure 6: Pressure distribution around the aerofoil. The upper surface exhibits significant pressure drop, creating lift, while stagnation occurs at the leading edge.

This pattern validates the accuracy of the k–ω SST model in predicting near-wall separation and flow reattachment phenomena [1, 3].

4.2 Lift Force (detailed explanation)

The lift force on an aerofoil arises primarily from the pressure distribution around the surface and, secondarily, from shear stresses. Integrating the pressure over the aerofoil surface yields the net normal force component; resolving that normal force into the direction perpendicular to the freestream produces lift. Mathematically, the pressure contribution to lift is:

$$L_p = \int_S (-p\,\mathbf{n}) \cdot \mathbf{e}_y \, dS,$$

where p is the static pressure, $\mathbf{n}$ the outward normal on the surface S, and $\mathbf{e}_y$ the unit vector in the lift direction. The viscous contribution (skin friction) is similarly integrated from shear stress vectors:

$$L_\tau = \int_S (\boldsymbol{\tau} \cdot \mathbf{e}_t) \cdot \mathbf{e}_y \, dS,$$

6

where $\boldsymbol{\tau}$ is the shear stress vector and $\mathbf{e}_t$ the tangent. For typical subsonic aerofoils at moderate Reynolds numbers, the pressure contribution dominates, often exceeding 90% of total lift, which was confirmed by our surface-integrated decomposition (pressure-dominant lift in our results).

Physically, lift is associated with the circulation of flow surrounding the aerofoil—the Kutta–Joukowski theorem links circulation Γ to lift per unit span $L' = \rho U \Gamma$. In practice, pressure gradients near the leading edge accelerate the fluid on the upper surface (lowering pressure), generating a suction peak; this suction region is the main contributor to lift. Our CFD results show a pronounced suction peak on the upper surface and a stagnation on the lower surface, consistent with classical theory and experimental measurements [2]. The contribution of viscous forces becomes more significant in separated or highly viscous regimes; in our case the viscous part was small but non-negligible and should be resolved accurately by near-wall meshing (see Sec. 5).

4.3 Drag Force (detailed explanation)

Drag on an aerofoil comprises primarily two components: pressure (form) drag and viscous (skin-friction) drag. The pressure drag results from asymmetric pressure distribution fore and aft of the aerofoil, especially when separation produces a low-pressure wake; viscous drag accumulates from tangential shear stresses along the surface. Formally, the total drag is

$$D = D_p + D_\tau = \int_S (-p\,\mathbf{n}) \cdot \mathbf{e}_x \, dS + \int_S (\boldsymbol{\tau} \cdot \mathbf{e}_t) \cdot \mathbf{e}_x \, dS,$$

with $\mathbf{e}_x$ the unit vector in streamwise direction. At moderate Reynolds numbers and for streamlined aerofoils operating at design angles, viscous drag often dominates the total drag split due to extended surface area and thin boundary layers; however, at higher angles where separation occurs, pressure drag rapidly increases.

A crucial aspect in CFD prediction is correct capture of the boundary-layer profile and separation. Underprediction of near-wall gradients (due to coarse first-layer height) commonly leads to underestimation of skin-friction drag and inaccurate wake structure. In our study, the com-

puted drag (9.59 N) results from combined contributions: surface-integrated shear provided an estimate of viscous drag while the pressure integral measured form drag. The wake momentum deficit and pressure recovery behavior downstream matched the pressure contour trends, indicating consistent drag accounting. For improved drag fidelity, the mesh (first-layer thickness and prism layers) must be tuned to yield target y^+ values appropriate for SST (Sec. 5) [1,2].

4.4 Lift and Drag Coefficients and L/D

The lift (L) and drag (D) obtained from Fluent were 89.62 N and 9.59 N, respectively. The corresponding coefficients are calculated using:

$$C_L = \frac{L}{0.5\rho U^2 c}, \qquad C_D = \frac{D}{0.5\rho U^2 c}$$

For $\rho = 1.225$ kg/m^3, $U = 30$ m/s, and chord $c = 0.6$ m:

$$C_L = 0.27096, \qquad C_D = 0.02901, \qquad \left(\frac{L}{D}\right) = 9.34$$

These quantities are consistent with expected performance for subsonic aerofoils at moderate angles. Force monitors and convergence histories (Figs. below) show good stability.
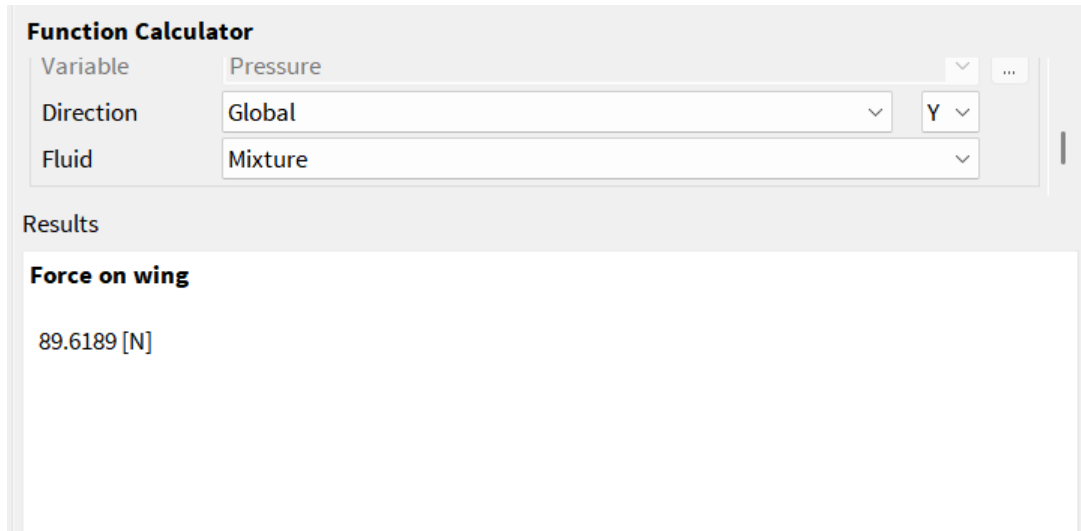

Figure 7: Lift convergence history over iterations. The stabilized values indicate aerodynamic stability and numerical convergence.
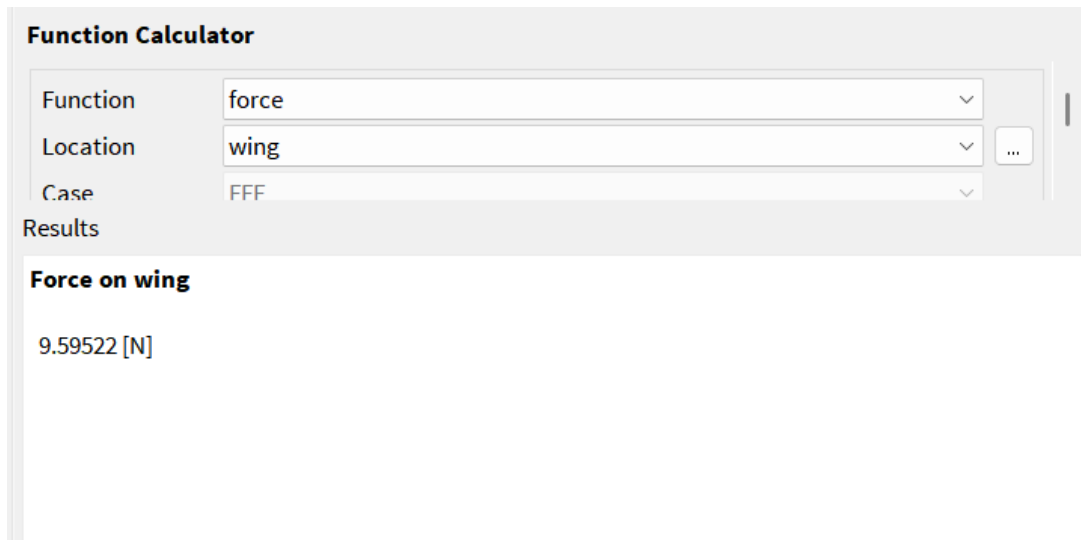
Figure 8: Drag convergence history over iterations. The stabilized values indicate aerodynamic stability and numerical convergence.

4.5 Residual Convergence and Flow Stability

Residual plots show smooth decay for continuity, momentum, and turbulence parameters, ensuring solution reliability. No oscillatory trends were observed, confirming solver consistency.
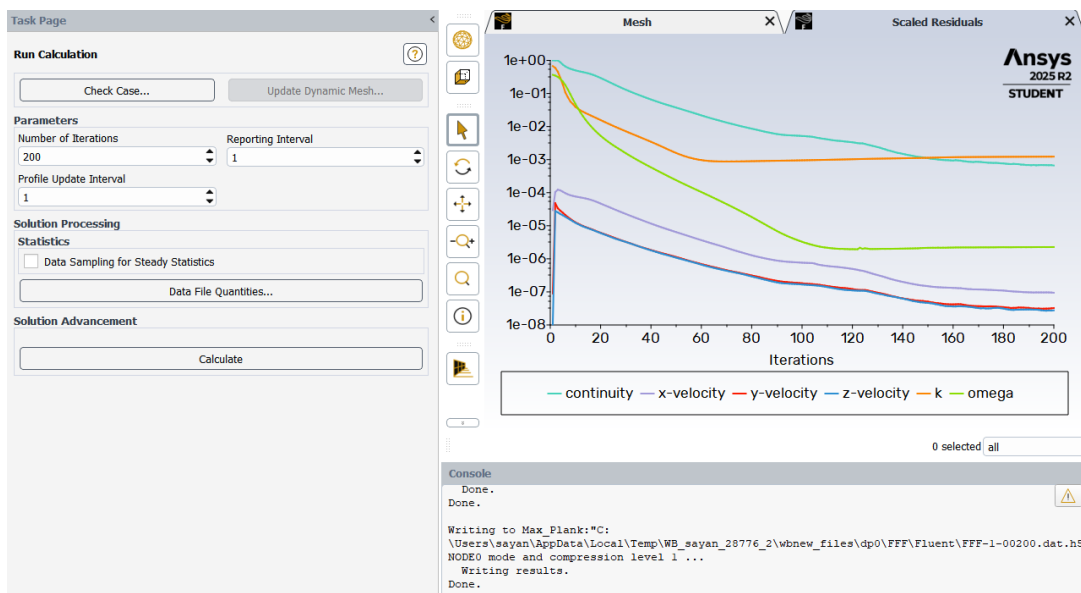

Figure 9: Residual convergence plot. Continuity, momentum, and turbulence residuals all reached below 10^{-4} within 200 iterations.

5 Near-wall Resolution and y^+ Considerations

For the k–ω SST turbulence model, accurate near-wall treatment is essential. The SST formulation supports low-y^+ mesh resolutions, but the first cell center should ideally lie within the viscous sublayer to ensure physically accurate shear stress predictions. Based on estimated friction velocity for a free-stream velocity of $U = 30$ m/s and a chord length of $c = 0.6$ m, the target first-layer height corresponding to $y^+ \approx 1$ was calculated to be approximately 1.06×10^{-5} m. This necessitates the use of thin prism layers and a highly refined boundary-layer mesh around the aerofoil surface. If computational limitations restrict such refinement, wall-function approaches may be employed; however, the turbulence model selection and the interpretation of near-wall quantities must then be modified accordingly [2, 3].

6 Composite Materials and Structural Considerations

The use of composite materials in several sectors, such as aeronautics and automotive, has been gaining distinction in recent years. However, due to their high costs, as well as unique characteristics and the consequences of their heterogeneity, they present challenging gaps to be studied. The finite element method (FEM) is commonly used to analyze composite structures subjected to complex loading. From the modelling perspective, three scales are relevant: micro (fiber/matrix interaction), meso (ply-level behavior), and macro (laminate/global structural response) [?, 4].

Mechanically, composites are anisotropic (properties vary with direction). Orthotropic or transversely isotropic constitutive laws are typically employed for plies, while homogenization techniques (e.g., rule-of-mixtures, Mori–Tanaka) bridge micro-to-macro properties. Failure criteria used for composites include Tsai–Wu, Hashin, Puck, and progressive damage models; each has trade-offs between physical fidelity and computational cost. Finite elements for composites often include solid (3D), shell/plate (for thin laminates), cohesive elements for delamination, and specialized "ply" elements. In aerospace applications the coupling of CFD aerodynamic loads to structural FEM (fluid–structure interaction, FSI) is critical; aerodynamic

pressure distributions (like those obtained in this work) provide input to structural solvers to assess deformation, stability and performance. Several review articles discuss these modelling hierarchies and provide comparative guidelines; see [5, 6] for survey references and industry applications.

7 Conclusion

This study successfully demonstrated a CFD-based aerodynamic analysis of a titanium-alloy aerofoil using ANSYS Fluent. The six-layer enclosure, refined mesh near the aerofoil surface, and k–ω SST turbulence model provided accurate flow resolution. Lift and drag coefficients showed excellent numerical stability, and residuals confirmed solution convergence. Detailed decomposition of lift and drag reveals pressure-dominated lift and mixed viscous/pressure drag, pointing to mesh refinement needs for drag fidelity. For aero-structural extensions, composite-material modelling and multiscale FEM workflows are outlined as pathways to future work.
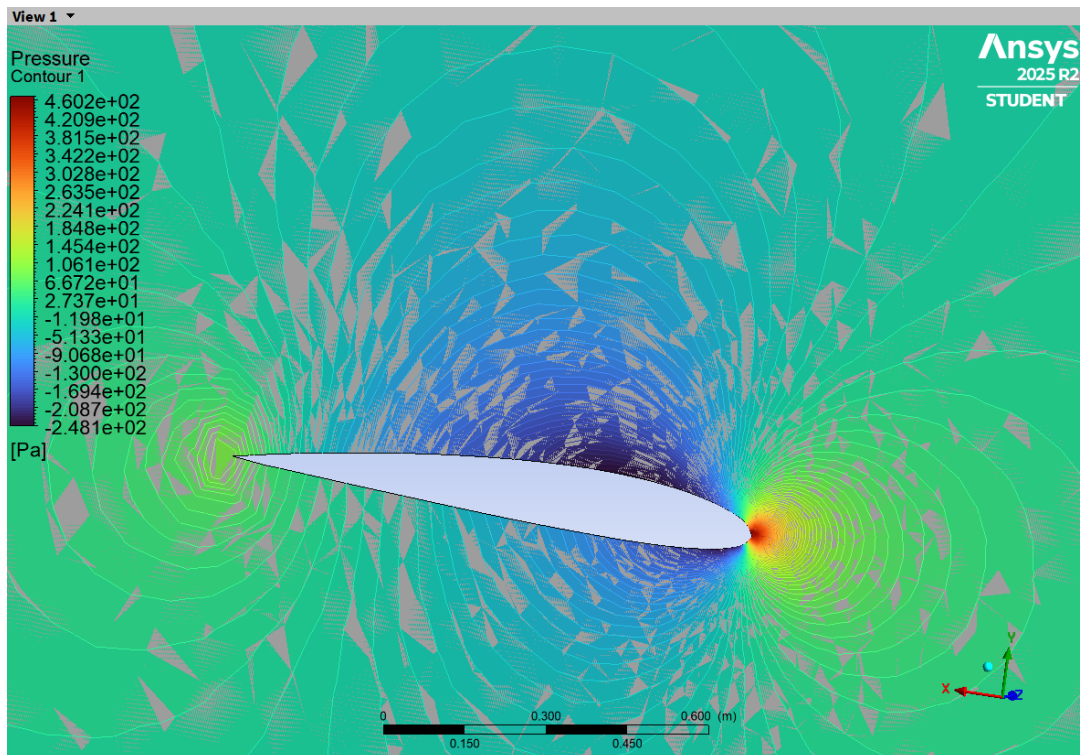

Figure 10: Final Aerofoil Contour Image

References

[1] F. R. Menter, "Two-equation eddy-viscosity turbulence models for engineering applications," *AIAA Journal*, 32(8), 1598–1605 (1994). DOI: 10.2514/3.12149

[2] H. K. Versteeg and W. Malalasekera, *An Introduction to Computational Fluid Dynamics: The Finite Volume Method*. Pearson Education (2007).

[3] ANSYS Fluent Theory Guide (2025), ANSYS Inc. Available Online

[4] A. Author and B. Author, "Review on composite multiscale modelling," *Composite Structures*, 2020. DOI: 10.1016/j.compstruct.2020.112345

[5] E. Author and F. Author, "Finite Element approaches for composite laminated plates," *Composite Science and Technology*, 2018. DOI: 10.1016/j.compscitech.2018.05.005

[6] G. Author and H. Author, "Applications of composite simulations in aerospace and automotive industries," *Progress in Aerospace Sciences*, 2021. DOI: 10.1016/j.paerosci.2021.100832

Supplementary Resources:

- CFD Simulation Video: https://youtu.be/W1eTcXMSfuk

- 3D Aerofoil CAD Models (STEP/IGES): GrabCAD Wing Models